



PII S0016-7037(00)00541-X

Apparent gibbsite growth ages for regolith in the Georgia Piedmont

PAUL A. SCHROEDER,^{1,*} NATHAN D. MELEAR,¹ PAUL BIERMAN,² MICHAEL KASHGARIAN,³ and MARC W. CAFFEE³¹Department of Geology, 210 Field St., University of Georgia, Athens, Georgia 30602-2501, USA²Department of Geology, Perkins Hall, University of Vermont, Burlington, Vermont 05405-0122, USA³Lawrence Livermore National Laboratory, 7000 East Ave., Livermore, California 94550-9234, USA

(Received December 29, 1999; accepted in revised form September 14, 2000)

Abstract—Carbon bound in gibbsite, collected from a residual weathering profile developed on a Paleozoic granite in the Georgia Piedmont, was examined for its ¹⁴C content and found to be geologically young. The study site, located at the Panola Mountain Research Watershed, has developed a granite–saprolite–soil regolith in which ¹⁴C-gibbsite model ages deep within the profile (C-horizon) average about 8000 years. Near the surface (A- and B-horizon) ¹⁴C-gibbsite model ages range from 2100 to 4200 years. Quartz has acquired ²⁶Al and ¹⁰Be inventories suggesting a near-surface residence time of at least 90,000 years. This age disparity supports the notion that secondary minerals undergo significant recrystallization as weathering fronts propagate into the landscape. Combining the results of ¹⁴C, ²⁶Al, and ¹⁰Be analyses offers the potential to assess differential rates of chemical weathering and continental denudation to understand better the links between rates of silicate rock weathering, climate, and soil residence times. Copyright © 2001 Elsevier Science Ltd

1. INTRODUCTION

Global rates of chemical weathering are intimately linked to the denudation of silicate terrains in humid-temperate to tropical climates (Berner and Berner, 1997). This link provides an important feedback to the abundance of atmospheric CO₂ (i.e., climate) as bicarbonate production returns carbon to the oceans (Berner, 1994). One valuable approach to constraining land surface denudation rates (mass loss per unit time) is the use of in situ produced cosmogenic nuclides such as ¹⁰Be and ²⁶Al (e.g., Bierman, 1994; Granger et al., 1996; Nishiizumi et al., 1991). For example, measuring the abundance of these isotopes in granites and granitic saprolite allows for an assessment of the length of time over which a weathering profile has been exposed to the surface (Bierman et al., 1995; Bierman, 1993). Near-surface mineral residence times, rates of mineral dissolution, and colluvial export rates are key parameters that are needed to understand the connection between climate change and landscape change.

One facet of the complex process of landscape evolution and denudation that has been difficult to measure is the timescale over which secondary minerals form. Knowledge about the duration and timing of secondary mineral formation offers insights into the pathways of mineral genesis and the “metabolic” properties of weathering profiles (e.g., long-term soil respiration rates and estimates of mass loss). This article introduces a new approach for estimating the relative age of secondary mineral authigenesis with the intent of better understanding models for the breakdown of silicate regolith in humid-temperate to tropical climates.

2. MATERIALS AND METHODS

A soil–saprolite–rock sequence was collected from the Panola Mountain Research Watershed (PMRW) operated by United States Geological Survey (USGS) in the Georgia Piedmont of the southeast-

ern United States (Huntington et al., 1993; Stonestrom et al., 1998) (Fig. 1). The bedrock is dominated by the Panola Granite, which has a very homogeneous, medium-grain, biotite–oligoclase–quartz–microcline composition with no discernible foliation (Melear, 1998). Samples were collected at a summit site in the PMRW where the weathering profile is believed to be wholly residual (i.e., not colluvial). The same sample suite was recently studied for its mineralogical, chemical, and stable carbon isotopic properties (Schroeder and Melear, 1999; Melear, 1998).

Samples analyzed for ¹⁰Be and ²⁶Al were taken from a soil pit at depths ranging from 2 to 10 cm below the surface. Samples were chemically and physically separated at the University of Vermont to produce >40 g of pure quartz by using a technique modified from Kohl and Nishiizumi (1992). Subsequent treatment involved HF dissolution of the quartz and the preparation of BeO and Al₂O₃ targets for AMS analysis (Bierman and Gillespie, 1997). All targets were analyzed by Accelerator Mass Spectrometry (AMS) at the Lawrence Livermore National Laboratory (Davies et al., 1990).

Procedures for extraction of CO₂ from the soil minerals, calcite and goethite, for paleoclimate studies have been developed and applied by Cerling (1984) and Yapp and Poths (1991). More recently, it was recognized that gibbsite sequesters carbon as it crystallizes in the soil–saprolite. This carbon is released as CO₂ as the gibbsite thermally breaks down at 230°C to 240°C under vacuum in the laboratory. We used a modified version of the method developed by Yapp and Poths (1991) and Schroeder and Melear (1999).

Five samples were selected for ¹⁴C measurements. Pretreatments included particle size separation (<2 μm retained), repeated digestions in 30% H₂O₂ and low-temperature (200°C) O₂ combustion to remove organic matter. Stable carbon isotopic analyses were conducted at the University of Georgia Stable Isotope Facility. CO₂ produced from the breakdown of gibbsite was cryogenically trapped into break-seal tubes and sent to the LLNL AMS facility, where graphite targets were prepared and analyzed. Line blanks were run to ascertain the contributions of ¹⁴CO₂ from other phases such as kaolin group minerals and from the extraction line itself. The 8720-year age of the kaolin blank has limited meaning because negligible gas was extracted (0.28 μmol CO₂ g⁻¹) compared with most samples. The low CO₂ yield is consistent with previous work by Schroeder and Melear (1999) who showed kaolin group minerals produced extremely little CO₂ during the 230°C treatment. The apparent ¹⁴C age of 45,710 years for the marble indicates that the extraction line is effectively devoid of external sources of ¹⁴C. Sample backgrounds have been subtracted on the basis of the measurements of the ¹⁴C-free marble. Backgrounds were scaled by relative sample size.

*Author to whom all correspondence should be addressed (schroe@gly.uga.edu).

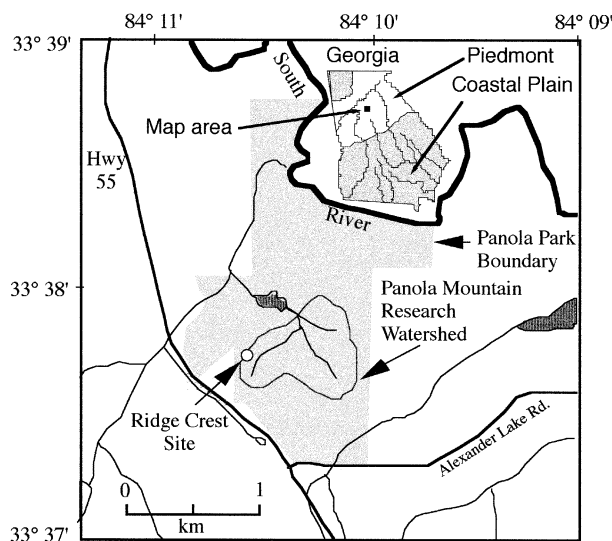


Fig. 1. Location map of the Panola Mountain Research Watershed. Gray area marks Panola Park boundary principally underlain by Panola Granite. Adapted from Huntington et al. (1993).

3. RESULTS

3.1. Cosmogenic ^{10}Be and ^{26}Al in Quartz

Large amounts of both ^{10}Be and ^{26}Al in quartz from three near-surface soil samples yielded an average of $5.26 \pm 0.04 \times 10^5$ and $2.94 \pm 0.06 \times 10^6$ atoms g^{-1} , respectively (Table 1). Although relatively large aliquots of quartz (41–57 g) and long counting times were used to generate precise data (average ratio 1σ uncertainty including blank correction = 1.8% for ^{10}Be and 2.2% for ^{26}Al), we can detect no systematic change of nuclide abundance over the top 10 cm of sampling. These data and others from deeper in the profile (Bierman et al., 1999) indicate that quartz grains over this depth are well mixed by bioturbation, pedogenesis, and/or cultivation and are thus isotopically homogeneous although some of the similarity may be due to the consistency of production rates over the uppermost 10 g cm^2 of soil or rock (Masarik and Reedy, 1995).

Although the measured abundances of in situ produced nuclides indicate relative surface stability and near-surface (≤ 2 m) residence times on the order of 10^5 years, uniquely quantifying such times is not possible because we do not know the exposure history of the quartz grains. Nevertheless, simple models can be used to constrain end-member exposure histories. Such models assume surface nuclide production rates of 6.5 atoms $^{10}\text{Be g quartz y}^{-1}$ and 39.7 atoms $^{26}\text{Al g quartz y}^{-1}$

at the sample site, elevation 260 m, and latitude $33^\circ 37'$. These rates are calculated from the production rate estimates of Nishiizumi et al. (1989) scaled only for neutrons (Lal, 1991).

If the sampled surface were exposed instantaneously by a deep (>2 m) erosion event and the nuclides were produced since that time without surface erosion, then model ^{10}Be and ^{26}Al ages are 94 ± 1 ky and 88 ± 2 ky, respectively, assuming that the upper 40 cm of the profile ($\rho = 1.15 \text{ g cm}^{-2}$) is isotopically homogeneous due to earthworm borrowing, tree-throw, and past cultivation. These model ages represent the shortest amount of time that quartz would need to be exposed at earth's surface to acquire the nuclide inventory measured. However, such a rapid-exposure, no-erosion model is not realistic in this eroding hilltop location and thus underestimates near-surface residence time. The ratio of ^{26}Al to ^{10}Be (mean $^{26}\text{Al}/^{10}\text{Be} = 5.58 \pm 0.10$), and the position of the samples when plotted on the two-isotope diagram suggest that steady erosion rather than instantaneous exposure is a more realistic model by which to interpret the data. Quartz, which was once deeply buried, was exposed over time to increasing doses of cosmic radiation as erosion and dissolution removed material above it. Thus, the analyzed quartz integrates cosmic-ray exposure over time (depth) as mass was lost from above and the quartz effectively moved toward the surface.

Assuming that the uppermost 40 cm of the soil profile has a similar nuclide abundance (N) and is well stirred, one can use the formulation of Lal (1991) with surface production (P_{eff} , atom g^{-1}) to model a steady-state rate of mass loss (m , $\text{g cm}^{-2} \text{ y}^{-1}$) from the soil profile assuming a characteristic neutron attenuation length (Λ) of 165 g cm^{-2} .

$$N = P_{\text{eff}}/(m/\Lambda + \lambda) \quad (1)$$

λ is the decay constant for the nuclides ^{26}Al and ^{10}Be ($9.9 \times 10^{-7} \text{ yr}^{-1}$ and $4.6 \times 10^{-7} \text{ yr}^{-1}$, respectively).

This model suggests that the PMRW ridge top we sampled is losing mass at a rate of $2.08 \times 10^{-3} \text{ g cm}^{-2} \text{ y}^{-1}$ (^{26}Al) and $1.98 \times 10^{-3} \text{ g cm}^{-2} \text{ y}^{-1}$ (^{10}Be). Translating mass loss rates to surface lowering rates is not straightforward because density changes with depth from 1.12 g cm^{-2} at the surface to 1.54 g cm^{-2} at a depth of 150 cm. Assuming an average density of 1.3 g cm^{-2} over the uppermost 2 m of the soil-saprolite profile, the calculated lowering rates of 15.2 ± 0.1 (^{10}Be) to $16.0 \pm 0.4 \text{ m My}^{-1}$ (^{26}Al) are equivalent to residence times over the uppermost 2 m ≈ 125 ky. If there is significant quartz enrichment by selective weathering of other phases, whole rock mass loss rates could be higher and residence times lower. These rates from the PMRW site are consistent with independent estimates for lowering rates of the Virginia Piedmont made by Pavich et al. (1985) using ^{10}Be adsorbed to clay minerals.

Table 1. Cosmogenic nuclide abundances in the quartz fraction of surface samples at the Panola Mountain ridge crest site.

Sample ID Panola Pit #1	Depth (cm)	Bulk density (g cm^{-3})	^{10}Be ($\times 10^5$ at g^{-1} quartz) ^a	^{26}Al ($\times 10^6$ at g^{-1} quartz) ^a	$^{26}\text{Al}/^{10}\text{Be}$
PP1-2	2	1.12	5.30 ± 0.14	3.00 ± 0.08	5.65 ± 0.22
PP1-3	6	1.15	5.22 ± 0.14	2.94 ± 0.09	5.63 ± 0.23
PP1-4	10	1.17	5.27 ± 0.15	2.88 ± 0.08	5.46 ± 0.22
Average ($\pm 1\sigma$)		1.15	5.26 ± 0.04	2.94 ± 0.06	5.58 ± 0.10

^a Errors propagated from both AMS and stable nuclide measurements.

Table 2. Carbon yields from gibbsite dehydroxylation and $\delta^{13}\text{C}$ and ^{14}C results for the $<2\text{-}\mu\text{m}$ sample fractions at the Panola Mountain ridge crest site.

Sample ID Panola Pit #1	Depth cm (horizon)	Sample mass (g)	CO_2 (μmol)	Yield ($\mu\text{mol g}^{-1}$ sample)	$\delta^{13}\text{C}$ (‰)	Graphite yield (mgC)	Model ^{14}C age ^c (yr)
PP1-3a	6 (A)	1.252	15.6	12.48	-11.6	0.19	3370 \pm 50
PP1-3b		1.379	17.0	12.35	-12.4	0.21	3710 \pm 50
PP1-3c		1.819	25.6	14.05	-12.0	0.31	3880 \pm 50
PP1-3					^a 12.96	^b -12.0	
PP1-5a	14 (B)	1.833	42.6	23.24	-13.2	0.50	3330 \pm 40
PP1-5b		1.143	25.6	22.37	-13.4	0.31	2120 \pm 40
PP1-5c		1.187	25.6	21.54	-13.7	0.29	2420 \pm 60
PP1-5					^a 22.38	^b -13.4	
PP1-6a	28 (B)	6.741	170.0	25.22	-14.7	1.04	4190 \pm 60
PP1-7a	51 (B)	1.274	29.8	23.39	-16.5	0.35	7480 \pm 50
PP1-7b		4.174	99.6	23.86	-16.8	0.71	8100 \pm 60
PP1-7				^a 23.63	^b -16.7		^b 7895 \pm 60
PP1-15a	236 (C)	1.260	8.5	6.75	-18.5	0.10	6590 \pm 80
PP1-15b		1.353	7.1	5.25	-20.7	^f	^f
PP1-15c		1.549	4.3	2.78	-19.4	0.07	9980 \pm 160
PP1-15					^a 4.92	^b -19.5	
Kaolin blank ^d		6.795	1.9	0.28	-	0.04	8720 \pm 240
Greek marble ^e		0.016	156.00	9750.00	2.7	0.93	45710 \pm 420

^a Average yield for replicate runs of separate aliquots a, b, c designated in column one.

^b Weighted average based on carbon yields.

^c Ages are radiocarbon years using the Libby half-life of 5568 years and following the conventions of Stuiver and Polach (1977).

^d Poorly ordered kaolin (Schroeder et al., 1998) processed using the same pretreatments as the PP samples.

^e Sample gas used as a line blank that was derived from H_3PO_4 digestion on CO_2 thermal extraction line.

^f Lost in transit.

3.2. Carbon Isotopes in Gibbsite

Stable carbon isotope analyses and ^{14}C abundances measured in CO_2 generated from the thermal breakdown of gibbsite depict an even more dynamic geochemical situation (Table 2). The trend of $\delta^{13}\text{C}$ values, ranging from -19.5 (1.0)‰ at depth (239 cm) to -12.0 (0.5)‰ near the surface (6 cm), is similar to the $\delta^{13}\text{C}$ values predicted for soil gas using the model of Cerling (1984). This model, which assumes diffusive transport of CO_2 in soil gases, has boundary conditions defined by the $\delta^{13}\text{C}$ of organic matter input to the soil (-24 ‰), preindustrial atmosphere (-6 ‰), and soil respiration rates of CO_2 ($9 \times 10^{-3} \text{ mol m}^{-2} \text{ h}^{-1}$) typical for a temperate forest at the latitude of the PMRW (Schroeder and Melear, 1999). The coincidence of the $\delta^{13}\text{C}$ trend and the model results suggests that the CO_2 sequestered by the gibbsite is recording an integrated history of the carbon flux through a slowly eroding profile.

Carbon derived from gibbsite contains only 29 to 77% of the ^{14}C found in modern carbon. This yields individual model ^{14}C ages that range from 2120 ± 40 to 9980 ± 160 yr, assuming ^{14}C was trapped by the gibbsite at one time. The high amount of ^{14}C in these samples shows that the carbon reservoir associated with gibbsite has incorporated or been open to exchange with atmospheric carbon during the past 20 to 40 ky; otherwise, the samples would be radiocarbon dead. Conversely, the gibbsite samples have lower $^{14}\text{C}/^{12}\text{C}$ ratios than modern carbon, suggesting that at least some carbon must have been sequestered in gibbsite for thousands of years. Wang et al. (1994) discuss the potential for the $^{14}\text{CO}_2$ content to be skewed

to a more enriched state (i.e., isotopically heavier) because the atmospheric component of the CO_2 flux is dominated by the root respiration component (as opposed to the flux from bacterial decomposition of soil organic matter). For the purpose of our study, we assume that the long-term flux of CO_2 is dominated by the soil organic matter decomposition component. The effect of this assumption is to produce minimum model ^{14}C ages.

Calculating gibbsite model ^{14}C ages from measured ^{14}C abundances requires two fundamental assumptions: (1) the initial ^{14}C content of carbon incorporated in the gibbsite structure is known and constant and (2) gibbsite has remained closed to carbon exchange since it was formed. The first assumption is reasonable given the short residence time (10^1 – 10^2 yr) for soil organic matter in the warm, humid southeastern United States (Raich and Schlesinger, 1992). The second assumption is almost certainly violated as discussed below. At this point, a distinction must be made between isotopic exchange between two intact mineral species and exchange due to dissolution and precipitation. Crystal-chemical evidence from coexisting goethite in the profile suggests that, near the surface, dissolution and precipitation of the hydroxides is a dominant reaction mechanism in the history of the secondary minerals in this study site (Melear, 1998). This is seen in Figure 2, where the crystallite size and degree of Al-substitution in goethite varies as a function of depth. For the case of the older ^{14}C model ages at depth, a closed system assumption might be supported where incipient hydroxide formation occurs in the absence of dissolution and precipitation reactions.

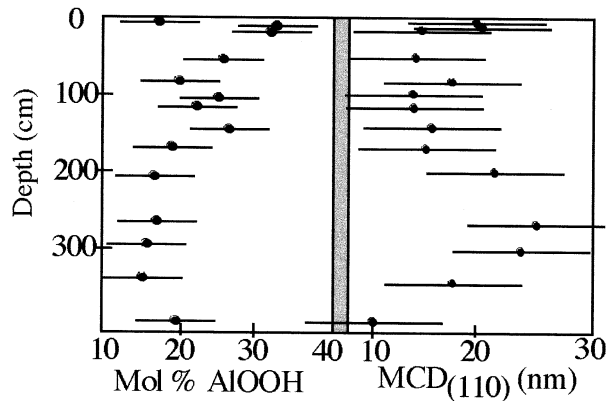


Fig. 2. Crystal chemistry of goethite in granitic soil-saprolite weathering profile from Panola Mountain. The left plot shows the degree of Al substitution in goethite, and the right side shows the mean coherent scattering domain (MCD) of the goethite (110) reflection. Error bars show precision of measurement, which is based on X-ray diffraction (modified from Melear, 1998).

Thus, the model or apparent ^{14}C ages calculated for gibbsite-bound carbon are similar to mean residence ages for authigenic minerals in the soil-saprolite; they reflect the mixture of various components of different ^{14}C abundances. Because of the short half-life of ^{14}C , mixing models are nonlinear precluding unique solutions. Nevertheless, the decrease with depth of gibbsite ^{14}C content (Fig. 3) that has been measured is an important and fundamental observation.

Both the individual model ^{14}C ages and the weighted-average ^{14}C ages of replicates generally increase with depth in the

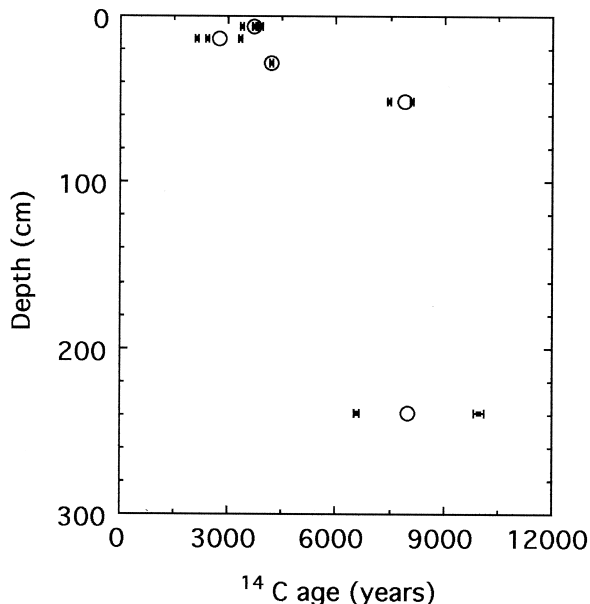


Fig. 3. Plot of gibbsite growth ages versus depth in residual weathering profile at the Panola Mountain Research Watershed located in the Georgia Piedmont. Data points at the same depth represent replicate runs. Error bars show analytical precision (1σ) with the AMS method. Circles show weighted averages of all samples from a single depth based on CO_2 yield.

profile. The ranges observed in the replicate analyses of different sample aliquots exceed the analytical precision of the AMS method, ± 40 to ± 160 yr (shown as error bars in Figure 3). Schroeder and Melear (1999) note that the $\delta^{13}\text{C}$ composition of time-stepped CO_2 evolved from thermal breakdown of gibbsite is variable, particularly for the shallow samples. There is likely a link between the $\delta^{13}\text{C}$ variation and the variation of ^{14}C content.

4. DISCUSSION

Determining the "age" of landscape regolith in humid temperate climates is a complex issue because the mineral and organic components that define the soil-saprolite have origins that vary over both spatial and temporal scales. The Panola granite is Mississippian in age (Atkins and Higgins, 1980). The in situ produced ^{10}Be and ^{26}Al abundances in quartz indicate the regolith has been residing near the surface for $\approx 10^5$ yr. Until now, the age of the authigenic mineral assemblages in soil has been largely unconstrained. Previous studies have used meteoric ^{10}Be to date soil weathering profiles (e.g., Pavich et al., 1985) by assuming that ^{10}Be was immobilized on clay surfaces, but others have raised questions about the mobility of ^{10}Be in weathering profiles (e.g., Monaghan et al., 1983).

^{14}C measurements made in the present study are indicative of the timescales over which gibbsite crystallization occurs within a weathering profile. The exact mechanism for carbon sequestration in gibbsite is not well understood, but it has been proposed that the gibbsite structure can harbor CO_3^- groups along hydroxyl edge defect sites that require excess charge compensation (Schroeder and Melear, 1999). Carbonate anions have a strong affinity for Al^{3+} and can displace H_2O and OH^- ligands (White and Hen, 1975).

The distribution of gibbsite model ^{14}C ages in the PMRW weathering profile therefore needs explanation in the context of models for silicate weathering and pedogenesis in humid-temperate climates. On the basis of crystal-chemical evidence seen in several granitic weathering profiles, Melear (1998) proposes that goethite assemblages in the regolith of Georgia Piedmont result from multigenerational recrystallization involving both the release of iron from primary phases and the recycling of previously formed secondary iron minerals. The depth-related trends in aluminum substitution and crystallinity suggest that goethite (and perhaps gibbsite) in the saprolite change as the land surface is lowered and the saprolite is transformed into soil.

Initial authigenic secondary minerals form deep within the saprolite near the incipient weathering front. Subsequent modification of this initial secondary mineral assemblage higher in the profile is attributed to changes in geochemical conditions, such as higher Al^{3+} and H^+ activities and lower Si^{4+} activity. Biologic activity increases as saprolite previously in the C-horizon is now affected by pedogenic processes in the B-horizon (Stonestrom et al., 1998). Enhanced biologic activity is a particularly important component of crystallization because dissolution of secondary iron minerals in oxidized near-surface environments must involve chelation by organic ligands produced mainly by microorganisms and/or localized reductive dissolution in the rhizosphere (Schwertmann, 1991). The net effect of these processes is a mineral assemblage composed of kaolinite, gibbsite, hydroxy-interlayered vermiculite, and

highly aluminous iron oxides. This assemblage is likely the result of solid-state transformations and dissolution or precipitation reactions involving secondary minerals formed earlier in the weathering process.

Assuming that the ridge crest site at PMRW is developing in a steady-state balance of downward chemical weathering, radioisotope incorporation and decay, surface erosion and regional uplift, then the mean residence ^{14}C ages of authigenic gibbsite in the weathering profile should reflect these complexities. The oldest model age of 9980 yr for the sample at 236 cm provides a minimum age for the time of initial gibbsite crystallization. The intermediate age of 4190 yr at 50-cm depth results from the coexistence of more newly formed recrystallized gibbsite and older inherited gibbsite. The youngest age of 2120 yr for samples in the upper B-horizon indicates significant recrystallization of preexisting gibbsite and/or newer gibbsite formed at the expense of other secondary minerals such as halloysite and kaolinite. The range of ages from 3370 to 3880 yr measured for gibbsite in the A-horizon reflects a complex mixture of inherited material and perhaps the loss of recently formed gibbsite by dissolution. Older model ^{14}C ages might occur below 236 cm (no deeper ^{14}C measurements were made), but our conceptual model predicts that at the incipient weathering front the “youngest” gibbsite population is forming today. This is a testable hypothesis.

An alternate explanation for the general trend of older model ^{14}C ages at depth and younger model ^{14}C ages near the surface (Fig. 3) could be a faster addition of gibbsite higher in the profile. This trend of model ^{14}C ages is seen in bulk soil organic matter at Panola Mountain (Nixon, 1981). Four radiocarbon dates from his study range from ≈ 5000 to 8000 yr BP, with a trend of increasing age with depth (0–1.2 m). These samples, however, are from a nearby aggradational (colluvial) soil profile; therefore, a direct comparison to the residual samples from our eroding study site is not meaningful. This increasing age and depth trend is common in the bulk soil organic matter of many soil profiles, with the explanation being that organic matter is added at a much higher rate near the surface.

Yet a third explanation for the variation in isotopic trends is resetting by isotopic exchange with no new formation of gibbsite. The strong bonding of carbonate anions to Al^{3+} , as discussed by White and Hen (1975), and the low temperatures at which gibbsite forms would argue against this explanation. Given the lack of experimental studies to test this hypothesis, little can be said at this point in time to support or refute isotopic exchange.

We advocate that the model ^{14}C ages measured in gibbsite from Panola Mountain are the net result of a multigenerational process that include a complex population of minerals. These minerals contain components of primary, inherited-secondary, and in situ-secondary phases or tertiary minerals (e.g., see Schroeder et al., 2000). This analysis does not consider the effects of translocating materials downward in the profile. Fine-grained, newly recrystallized gibbsite moving downward into the B-horizon would also lead to the observed trend of slightly younger model ages in the B-horizon.

5. CONCLUSIONS

CO_2 produced during the laboratory thermal breakdown of regolith-derived gibbsite has measurable abundances of cosmo-

genic ^{14}C . This carbon is sequestered from soil gases by gibbsite as it crystallizes, and its $\delta^{13}\text{C}$ composition is similar to the predicted $\delta^{13}\text{C}$ composition of soil-respired CO_2 (Schroeder and Melear, 1999). The mean residence ^{14}C age of the gibbsite deep in the weathering profile (C-horizon) at PMRW suggests mineralization 6,500 to 10,000 yr ago. Samples from the A- and B-horizons have much younger model ages, 2100 to 4200 ^{14}C years. ^{14}C abundances as a function of depth support the notion that gibbsite undergoes significant recrystallization as weathering fronts propagate downward into the landscape. ^{26}Al and ^{10}Be analyses of surface samples constrain the residence time of residual quartz in the uppermost soil to $\geq 90,000$ yr, suggesting that quartz grains linger longer than gibbsite. The combination of the cosmogenic isotopes, studied in samples from the PMRW, shows a new approach to evaluating rates of chemical and physical mass loss from silicate terrains in humid temperate climates.

Issues that require further study include the following: (1) the mechanism of carbon sequestration into hydroxide minerals and the crystallographic association of carbon with the gibbsite structure, (2) the nature of cosmogenic nuclide abundances throughout the entire weathering profile, and (3) the application of these methodologies to the study of paleosols and other residual weathering profiles in different climates and lithologic settings.

Acknowledgments—The carbon isotope work was supported by a grant to the senior author from the NSF-Geologic Record of Global Change Program (EAR9628035). The cosmogenic isotope work was supported by a grant to Bierman from the NSF-Hydrologic Sciences Program (EAR9628559). We thank Bill McClain, Nancy Chapman (Howard Hughes Medical Institute-Undergraduate Research Apprentice Program), and Susan Nies for sample processing. The reviews of Crayton Yapp, Jay Quade, and Darryl Granger edited the manuscript. Radiocarbon analyses were performed under the auspices of the U.S. Department of Energy by Lawrence Livermore National Laboratory (contracts W-7405-Eng-48 and DOE Eqn. 6-7405).

Associate editor: T. E. Cerling

REFERENCES

- Atkins R. L. and Higgins M. W. (1980) Superimposed folding and its bearing on geologic history of the Atlanta, Georgia area. In *Excursions in Southeastern Geology* (ed. R. W. Frey), Vol. I, pp. 19–40. American Geological Institute.
- Berner R. A. (1994) GEOCARB II: A revised model of atmospheric CO_2 over Phanerozoic time. *Am. J. Sci.* **294**, 56–91.
- Berner R. A. and Berner E. K. (1997) Silicate weathering and climate. In *Tectonic Uplift and Climate Change* (ed. W. F. Ruddiman), pp. 354–365. Plenum Press.
- Bierman P. R. (1994) Using in situ produced cosmogenic isotopes to estimate rates of landscape evolution; a review from the geomorphic perspective. *J. Geophysical Res., B, Solid Earth and Planets* **99**, pp. 13,885–13,896.
- Bierman P. (1993) Cosmogenic isotopes and the evolution of granitic landforms. Ph. D. thesis, Univ Washington Seattle, 268 p.
- Bierman P., Clapp E., Caffee M., and Schroeder P. (1999) Understanding earth surface processes with 10-Be (and a little 26-Al). *Geol. Soc. Amer. Abstr Programs*, **31**, 7, A-305.
- Bierman P. and Gillespie A. (1997) Short course notes for “Geomorphologic application of cosmogenic isotopes.” *Geological Society of America annual meeting*, Seattle, WA., 112 p.
- Bierman P., Gillespie A., Caffee M., and Elmore D. (1995) Estimating erosion rates and exposure ages with ^{36}Cl produced by neutron activation. *Geochim. Cosmochim. Acta* **59**, 3779–3798.
- Cerling T. E. (1984) The stable isotopic composition of modern soil

- carbonate and its relationship to climate. *Earth Planet. Sci. Lett.* **71**, 229–240.
- Davies J. S., Proctor I. D., Southon J. R., Caffee M. W., Heikkinen D., Roberts M. L., Moore T. L., Turteltaub K. W., Nelson D. E., Loyd D. H., and Vogal J. S. (1990) LLNC/UC AMS facility and research programs. *Nuclear Instruments and Methods in Physics* **B52**, 269–272.
- Granger D. E., Kirchner J. W., and Finkel R. (1996) Spatially averaged long-term erosion rates measured from in-situ produced cosmogenic nuclides in alluvial sediment. *J. Geol.* **104**, 249–257.
- Huntington T. G., Hooper R. P., Peters N. E., Bullen T. D., and Kendall C. (1993) Water, Energy and Biogeochemical Budgets investigation at Panola Mountain Research Watershed, Stockbridge, Georgia. U.S. Geological Survey Open File report 93-55.
- Kohl C. P. and Nishiizumi K. (1992) Chemical isolation of quartz for measurement of in-situ -produced cosmogenic nuclides. *Geochim. Cosmochim. Acta* **56**, 3583–3587.
- Lal D. (1991) Cosmic ray labeling of erosion surfaces: In situ production rates and erosion models. *Earth Planet. Sci. Lett.* **104**, 424–439.
- Masarik J. and Reedy R. C. (1995) Terrestrial cosmogenic-nuclide production systematics calculated from numerical simulations. *Earth Planet. Sci. Lett.* **136**, 381–396.
- Melear N. D. (1998) Crystal properties of goethite and hematite from three weathering profiles of the Georgia Piedmont. Ph.D. thesis, Univ. Georgia, Athens, p. 155.
- Monaghan M. C., Krishnaswami S., and Thomas J. H. (1983) ^{10}Be concentrations and the long-term fate of particle-reactive nuclides in five soil profiles from California. *Earth Planet. Sci. Lett.* **65**, 51–60.
- Nishiizumi K., Kohl C. P., Arnold J. R., Klein J., Fink D. and Middleton R. (1991) Cosmic ray produced ^{10}Be and ^{26}Al in Antarctic rocks: Exposure and erosion history. *Earth Planet. Sci. Lett.* **104**, 440–454.
- Nishiizumi K., Winterer E. L., Kohl C. P., Klein J., Middleton R., Lal D., and Arnold J. R. (1989) Cosmic ray production rates of ^{10}Be and ^{26}Al in quartz from glacially polished rocks. *J. Geophys. Res. B, Solid Earth and Planets* **94**, 17,907–17,915.
- Nixon R. A. (1981) Rates and mechanisms of chemical weathering in an organic environment at Panola Mountain, Georgia. Ph.D. thesis, Emory Univ. Atlanta, 172 p.
- Pavich M. J., Brown L., Valette-Silver J. N., Klein J., and Middleton R. (1985) ^{10}Be analysis of a Quaternary weathering profile in the Virginia Piedmont. *Geology* **13**, 39–41.
- Raich J.W. and Schlesinger W. H. (1992) The global carbon dioxide flux in soil respiration and its relation to vegetation and climate. *Tellus* **44B**, 81–99.
- Schroeder P. A., Melear N. D., West L. T., and Hamilton D. A. (2000) Meta-gabbro weathering in the Georgia Piedmont, USA: Implications for global silicate weathering rates. *Chem. Geol.* **163**, 235–245.
- Schroeder P. A. and Melear N. D. (1999) Stable carbon isotopic signatures preserved in authigenic gibbsite from a forested granitic regolith: Panola Mt., Georgia, USA. *Geoderma* **91**, 261–279.
- Schroeder P. A., Pruett R. J., and Hurst V. J. (1998) Effects of secondary iron phases on kaolinite ^{27}Al MAS NMR spectra: *Clays and Clay Minerals* **46**, 429–435.
- Schwertmann U. (1991) Solubility and dissolution of iron oxides. *Plant and Soil* **130**, 1–25.
- Stuiver M. and Polach H. A. (1977) Discussion; reporting of C-14 data. *Radiocarbon* **19**, 355–363.
- Stonestrom D. A., White A. F., and Akstin K. C. (1998) Determining rates of chemical weathering in soils—solute transport versus profile evolution. *J. Hydrol.* **209**, 331–345.
- Wang Y., Amundson R., and Trumbore S. (1994) A model for soil $^{14}\text{CO}_2$ and its implication for using ^{14}C to date pedogenic carbonate. *Geochim. Cosmochim. Acta* **58**, 393–399.
- White J. L. and Hen S. L. (1975) Role of carbonate in aluminum hydroxide gel established by Raman and IR analysis. *J. Pharm. Sci.* **64**, 264–265.
- Yapp C. J., and Poths H. (1991) $^{13}\text{C}/^{12}\text{C}$ ratios of the Fe(III) carbonate component in natural goethites. In *Stable Isotope Geochemistry: A Tribute to Samuel Epstein* (ed. H. P. Taylor, J. R. O'Neil, and I. R. Kaplan), pp. 257–270. The Geochemical Society.